arXiv:1905.06975v1 [cs.DC] 16 May 2019

Auto-tuning of dynamic load balancing applied to 3D reverse time migration on multicore systems

Ítalo A. S. Assis, João B. Fernandes, Tiago Barros, Samuel Xavier-de-Souza

December 15, 2024

Abstract

Reverse time migration (RTM) is an algorithm widely used in the oil and gas industry to process seismic data. It is a computationally intensive task that suits well in parallel computers. Because of it being massive and regular, this type of task is often equally and statically distributed among the available parallel workers. However, this strategy is often not optimal. When the workers are heterogeneous, and even when most have similar processing power, many of them might still have to wait idly for the slower workers. In this paper, we show that even small performance differences between homogeneous cores can considerably affect the overall performance of a 3D RTM application. We show that dynamic load distribution has a significant advantage over the conventional static distribution. However, the granularity of the dynamically distributed chunks of work plays a key role in harvesting this advantage. In order to find the optimal granularity, we propose a coupled simulated annealing (CSA) based auto-tuning strategy that adjusts the chunk size of work that OpenMP parallel loops assign dynamically to worker threads during the initialization of a 3D RTM application. Experiments performed on computational systems with different processor and RAM specifications and for different sizes of input show that the proposed method is consistently better than two default OpenMP loop schedulers being up to 44% faster.

keywords: Auto-tuning, Coupled simulated annealing, Reverse time migration, OpenMP, Load balancing

1 Introduction

Seismic reflection surveying is the best known and used geophysical method for subsurface imaging. Oil and gas exploration is likely its main application. Its main objective is to generate an image of a region of the subsurface to identify structures of interest.

Seismic data can go through several processing steps in order to improve the signal-to-noise ratio (SNR) and the resolution of the seismic image. One of the most important of these steps is migration, which is responsible for positioning seismic reflection events in their correct place when imaging the subsurface. In this context, reverse time migration (RTM) [1, 2] has been widely used as a migration technique, to more accurately take into account the wave propagation effects resulting in subsurface images with higher definition.

Simulating wave propagation comprises the majority of an RTM and is computationally intensive, especially for the three-dimensional case. Therefore, the computational cost is the main factor that limits the application of RTM, as well as for several other geophysical algorithms [3, 4]. For this reason, parallel computing techniques have been widely applied to these methods (e.g., [5]).

Load balancing is one of the main aspects to be considered in parallel applications. It can be defined as the distribution of the computational load among the available processing resources (e.g., cores, computing nodes). A way to perform load balancing is by dividing the workload in chunks of computation to be distributed among the computational resources either statically or dynamically.

Load balancing parallel seismic methods, such as RTM, is especially challenging with the rise of heterogeneous machines. Nevertheless, as we will see, even for homogeneous architectures, a static load balancing may not be optimal.

Auto-tuning techniques have been used as an approach to find near-optimal load balancing. Tchiboukdjian *et al.* [6] introduced a scheduler for applications with linear access to shared memory. They aim to improve locality by guaranteeing that all data in the cache are used before being replaced.

Furthermore, load balancing can also be used along with processors frequency control tools to improve the energy efficiency of imbalanced parallel applications in multicore systems, as shown by [7, 8]. Both these works use processors frequency scaling techniques to slow down less loaded cores in order to save energy.

In the context of seismic applications, some authors have developed auto-tuning techniques for the finite difference method (FDM), which is often used in geophysical applications. Katagiri *et al.* [9, 10] introduced ppOpen-AT, a framework for code optimization guided by directives. Barros *et al.* [11] provided experiments to show that the optimal load balancing for shared memory environments depends on the hardware and software employed. They also point to the coupled simulated annealing (CSA) [12] algorithm as a promising method to obtain a near-optimal load balance for a 3D FDM.

RTM has also been the target of auto-tuning techniques. Sena *et al.* [13] presented a method to determine a near-optimal block size by testing a set of possible values in a few time steps of RTM and choosing the one with the shortest execution time. Andreolli *et al.* [14, 15] introduce an approach to tune seismic applications automatically by compiling and running each set of parameters chosen by a genetic algorithm, including chunk size and compilation flags. According to [15], after all, code optimization is done, auto-tuning will become a necessary step to extract the best performance from computing systems.

We present an execution time CSA-based auto-tuning strategy for properly choosing the optimal chunk size that reduces the execution time of a 3D RTM algorithm. Our strategy aims to reduce the execution time of a 3D RTM by automatically finding an ideally optimal chunk size for OpenMP [16] parallel loops.

Following, we present the basics of our target application: the RTM (Section 2), the parallelization strategies made available by OpenMP (Section 3) and the optimization method that comprises the proposed auto-tuning, the CSA (Section 4). Then, we provide a detailed description of our RTM implementation (Section 5) as well as of the proposed auto-tuning approach (Section 6). Section 7 displays the results of the proposed method in comparison with the standard OpenMP schedules. Section 8 concludes this paper.

2 Reverse Time Migration Formulation

The seismic reflection method consists of three main steps: acquisition, processing, and interpretation of seismic data. In the acquisition, seismic shots, reflected by subsurface interfaces, are recorded at surface level by receivers. The signal recorded by each detector, from each seismic shot, is called a seismic trace. A set of seismic traces is called a seismogram. Seismograms can be converted to depth estimates of interfaces between different subsurface materials during processing.

After the acquisition step, several techniques can be used to process seismic data. In general, the purpose of processing reflection data is to increase the SNR and improve the vertical resolution of resulting seismic images. Migration is one of the main steps in the seismic data processing. It aims to 1) properly position seismic reflections at the coordinates of the reflector in the subsurface; 2) reduce diffraction effects in the images; 3) improve the spatial resolution.

Modern migration approaches use the seismic wave equation, a partial differential equation describing wave motion, generated by a source in a medium. The scalar equation for 3D acoustic waves is defined as

$$\frac{\partial^2 u(\mathbf{x})}{\partial x_1^2} + \frac{\partial^2 u(\mathbf{x})}{\partial x_2^2} + \frac{\partial^2 u(\mathbf{x})}{\partial x_3^2} = \frac{1}{c(\mathbf{x})^2}\frac{\partial^2 u(\mathbf{x})}{\partial t^2} + s(t), \tag{1}$$

where $\mathbf{x} = (x_1, x_2, x_3)$ are the spatial dimensions, $u(\mathbf{x})$ is the acoustic pressure, $c(\mathbf{x})$ is the propagation velocity and $s(t)$ is the source function at time t.

Spatial and time restrictions should be observed when solving finite differences by a numerical approach [17]. These restrictions are defined as:

$$\max(\Delta x_1, \Delta x_2, \Delta x_3) \leq \frac{c_{\min}}{W f_{\max}} \tag{2}$$

and

$$\Delta t \leq \frac{2\min(\Delta x_1, \Delta x_2, \Delta x_3)}{\pi c_{\max}\sqrt{3}}, \tag{3}$$

where Δx_1, Δx_2 and Δx_3 are the spatial sampling of dimensions x_1, x_2 and x_3, Δt is the time sampling; $f_{\max}$ is the maximum frequency of $s(t)$; $c_{\min}$ and $c_{\max}$ are the minimum and the maximum values of $c(\mathbf{x})$; and W is the number of grid points per minimum wavelength. According to [17], W must be equal

or greater than 4 for high order finite differences schemes. Non-compliance with (2) and (3) would result in numerical dispersion and instability.

Another important aspect is that the geological model encoded in $c(\mathbf{x})$ must be restricted to a finite number of points on a mesh, even though the Earth is heterogeneous and continuous. In order to represent real boundaries, it is common to apply artificial edges to the model limits, to absorb the energy reaching the borders [18].

There are several approaches to migrate seismic data. We use migration by finite differences (or wave equation migration), in which the wave equation is approximated by a finite-difference equation, suitable to be solved by a computer as explained above. One of the main migration methods by finite differences is RTM [1, 2]. In RTM, source and receiver wavefields are propagated forward and backward in time, respectively. RTM imaging relies on the physical property that those pressure waves must correlate at the reflective interfaces.

The core of an RTM can be divided into three stages. The first stage is the simulation of the propagation of a wave field resulting from the excitation of a seismic source. The second stage is the backpropagation of wavefields registered in a seismogram. Finally, the third stage is the imaging condition, which is a correlation between the forward and backward propagated wave fields and produces an image of the subsurface. This process is repeated for all the shots of seismic data available.

The propagation and backpropagation steps use the same velocity model shown in (1) as $c(\mathbf{x})$. This model specifies the wave velocity for each mesh point and represents the different properties of the materials and boundaries, in the volume being imaged.

In the imaging condition stage, the wavefields generated by the propagation of the source and the backpropagation of the observed data are correlated pointwise, at each time interval, to generate an image. Mathematically, it is defined as

$$I(\mathbf{x}) = \int_{t=0}^{T} u_{\mathrm{i}}(\mathbf{x}, t) \cdot u_{\mathrm{r}}(\mathbf{x}, t) \mathrm{d}t, \tag{4}$$

where $I(\mathbf{x})$ is the resulting image, $u_{\mathrm{i}}(\mathbf{x}, t)$ is the wavefield propagated with the source excitation, $u_{\mathrm{r}}(\mathbf{x}, t)$ is the wavefield of backpropagated data and T is the total simulation time. The migration of each seismic shot generates an image. These images are stacked to build the total migrated volume.

Each cycle of a seismic survey ends with the interpretation phase. Since both coverage and resolution are better with 3D data, these surveys lead to improvement of interpretation, compared with 2D surveys and are standard today [19].

3 Parallelization strategy

In this work, the RTM algorithm was implemented with two degrees of parallelization. The first is the migration of different common-shot (CS) gathers, i.e., seismic data with the same shot coordinates, which is implemented with message passing interface (MPI) [20], for distributed memory environments. The second is the migration of a single CS gather and is performed in shared memory environments, with OpenMP [16].

Our work is applied in the second degree of parallelization, where different loops of the RTM operation of each CS gather are parallelized among the cores of a multicore system, with OpenMP. This parallelization is performed by dividing each loop into loops of smaller sizes, which are computed in the different cores of the multicore system. The size of these smaller loops is usually referred to as the *chunk size*. The main goal of our work is to balance the computation of the smaller loops by the different cores, by choosing the proper chunk size, which is known as workload balancing. The proposed load balancing approach is discussed in more detail in Section 4.

For the parallelization with OpenMP, the *parallel for* construction was employed. This construction automatically distributes the workload (N_{loop}) among all threads (N_{threads}), in the loop where it is applied. The workload distribution within the threads can be changed by using the OpenMP clause *schedule* and variable *chunk size*. The different OpenMP workload distributions used in this work are explained next.

Static: is the standard distribution in OpenMP, where the load is distributed for each thread in fixed data blocks of roughly $N_{\text{loop}}/N_{\text{threads}}$. It is possible to choose the size of these blocks by changing the *chunk size* variable.

Dynamic: similar to the *static* one, with the main difference that, when a thread finishes to compute the work allocated to it and becomes idle, the system automatically allocates more work to this thread, until all the work finishes.

Auto: is the automatic distribution provided by OpenMP. It delegates all the scheduling decisions to the compiler.

4 Coupled simulated annealing

Coupled Simulated Annealing (CSA) [12] is a global optimization algorithm, based on the well-known simulated annealing (SA) algorithm [21]. The SA algorithm, also a global optimization method, is inspired by the thermodynamic annealing process, which consists of a heat treatment that alters the physical or chemical properties of a given material. The SA algorithm is employed in minimization (or maximization) problems, where the goal is to obtain the minimum (or maximum) of a specific cost function, namely the *energy* of the annealing process. Our work is focused solely on minimization problems.

Briefly, the SA algorithm is divided into the generation of new solutions and acceptance of these solutions. Algorithm parameters, known as generation and acceptance *temperatures*, control both these stages. The proper tuning of these temperatures is a considerable challenge when using SA-based algorithms. New possible solutions, also known as probe solutions, are generated by a function of the generation temperature. If a probe solution yields a smaller value of the cost function, this solution is accepted as the new one with probability one; otherwise, this solution is only accepted as the new one with the probability given by a function of the acceptance temperature.

In its turn, the CSA algorithm consists of a set of parallel SA algorithms, known as SA optimizers. Each SA optimizer generates and evaluates a probing solution, updating its current state. The generation and acceptance temperatures are equal for all the different SA instances. The main differences between CSA and SA are that 1) for accepting solutions with higher cost function values, the CSA considers all current solutions; and 2) the acceptance criterion is based on the current solutions and also on a *coupling* term between these solutions. The coupling approach has shown to be capable of reducing the sensitivity of the algorithm to initialization parameters and providing information that might steer the overall optimization process toward the global optimum.

The CSA algorithm employed in this work is the one described in [22,23], which is implemented as follows. Let $a_i \in \Theta$ and $b_i \in \Omega$ be, respectively, the current and probe solutions of the i-th SA optimizer; with Θ and Ω being the set of current and probe solutions, respectively, and $i = 1, \ldots, m$, where m is the number of elements in both Θ and Ω. At the k-th iteration of the

CSA algorithm, the probe solutions are given by

$$b_i = a_i + \epsilon_i T_k^{\text{gen}}, \tag{5}$$

where T_k^{gen} is the generation temperature and ϵ_i is a random variable sampled from the Cauchy distribution

$$g(\epsilon,\, T) = \frac{T}{(\epsilon^2 + T^2)^{(D+1)/2}}, \tag{6}$$

where $T = T_k^{\text{gen}}$ and D is the dimension of the problem. The rule for updating T_k^{gen} is also a free choice of the specific CSA implementation. We followed the guidelines from [22] and used as update $T_{k+1}^{\text{gen}} = 0.99999 T_k^{\text{gen}}$, with T_k^{gen} being updated to 99.999 % of its previous value.

Each solution, a_i and b_i, has an associated energy (or cost) value, $E(a_i)$ and $E(b_i)$. The acceptance probability function is defined as:

$$A_\Theta = \frac{\exp\left(\frac{E(a_i) - \max(E(a_i))_{a_i \in \Theta}}{T_k^{\text{ac}}}\right)}{\gamma}, \tag{7}$$

where T_k^{ac} is the acceptance temperature and γ is the coupling term, given by:

$$\gamma = \sum_{\forall a \in \Theta} \exp\left(\frac{E(a) - \max(E(a_i))_{a_i \in \Theta}}{T_k^{\text{ac}}}\right). \tag{8}$$

If $E(b_i) > E(a_i)$, a_i assumes the value of b_i only if $A_\Theta < r$, where r is a random variable sampled from an uniform distribution in the interval [0, 1]. Otherwise, if $E(b_i) < E(a_i)$, a_i assumes the value of b_i with probability one.

As shown in [12], the CSA performance is improved if the variance of A_Θ is kept close to its maximum value. This variance might be written as

$$\sigma^2 = \frac{1}{m} \sum_{\forall a \in \Theta} A_\Theta^2 - \frac{1}{m^2} \tag{9}$$

and lays in the interval

$$0 \leq \sigma^2 \leq \frac{m-1}{m^2}. \tag{10}$$

The controlling of this variance value can be accomplished by using the following rule to update the acceptance temperature:

$$T_{k+1}^{\text{ac}} = \begin{cases} T_k^{\text{ac}}(1-\alpha), & \text{if} \quad \sigma^2 < \sigma_D^2 \\ T_k^{\text{ac}}(1+\alpha), & \text{if} \quad \sigma^2 \geq \sigma_D^2 \end{cases}, \tag{11}$$

where σ_D^2 is the desired variance, which should be kept as close as possible to $\frac{m-1}{m^2}$, and α is the acceptance temperature modification rate, usually a value within the interval (0, 0.1].

The CSA algorithm is parameterized by setting the initial temperature values T_0^{gen} and T_0^{ac}. In this work, we determined these initial temperatures mostly by trial and error. However, we noticed in our experiments that the CSA algorithm is very robust to the initial values of the acceptance temperature, T_0^{ac}. In this work, the adopted stopping criterion for the CSA implementation was the total number of algorithm iterations, which was left to be set by the user and is represented by the variable N. There are several comparisons between CSA based optimization methods and other algorithms [12, 23], where one may see the main advantages in using CSA, mostly related to its robust initialization and functional capacity of finding values close to the global optimum. Due to these characteristics, the CSA seemed the right choice for the proposed auto-tuning algorithm.

In the proposed auto-tuning approach, the CSA is employed to minimize the execution time of different loops in the RTM algorithm, parallelized with OpenMP, by properly choosing the optimal workload chunk size of each OpenMP thread. Therefore, the cost function $E(a_i)$ is related to the execution time of an OpenMP *parallel for* construction and the variable a_i is related to the chunk size, in the *dynamic* OpenMP distribution.

5 Implementation aspects of RTM

The RTM program developed to test the proposed auto-tuning is implemented in C, using a hybrid parallel approach. MPI distributes shots among the nodes of a distributed memory system while OpenMP schedules chunks of the 3D mesh representing the spatial domain to cores of a shared memory system.

The wave propagator of our RTM implementation solves the wave equation by FDM, using an eighth order in space and second order in time stencil. We used non-reflecting boundary condition to absorb the energy at the boundaries as described in [18]. The absorbing boundary coefficients are

computed by

$$\phi(i) = \begin{cases} \pi f_{\text{peak}} \Delta t \left(\dfrac{w_{\text{i}}}{w_{\text{b}}} \right)^2, & \text{on the borders,} \\ 0, & \text{otherwise,} \end{cases} \tag{12}$$

$$\phi(\mathbf{x}) = \phi(x_1) + \phi(x_2) + \phi(x_3), \tag{13}$$

$$\phi_1(\mathbf{x}) = \frac{1}{1 + \phi(\mathbf{x})}, \tag{14}$$

$$\phi_2(\mathbf{x}) = 1 - \phi(\mathbf{x}), \tag{15}$$

where f_{peak} is the peak frequency of the source, w_{b} is the thickness of the absorbing boundary, in number of grid points, and w_{i} ranges from 0 to w_{b}, indicating the shortest distance from a point (x_1, x_2, x_3) to the border's interior edge. Note that, away from the borders, $\phi_1(\mathbf{x}) = \phi_2(\mathbf{x}) = 1$ and we recover the usual FDM solution.

Using a finite difference second order scheme in time and applying the coefficients of (14) and (15) to (1) leads to

$$u(\mathbf{x}, t + \Delta t) = \phi_1(\mathbf{x}) \cdot \Bigg\{ 2u(\mathbf{x}, t) - \phi_2(\mathbf{x}) \cdot u(\mathbf{x}, t - \Delta t) + (c(\mathbf{x})\Delta t)^2 \cdot \left[\frac{\partial^2 u(\mathbf{x})}{\partial x_1^2} + \frac{\partial^2 u(\mathbf{x})}{\partial x_2^2} + \frac{\partial^2 u(\mathbf{x})}{\partial x_3^2} - s(t) \right] \Bigg\}, \tag{16}$$

where the source $s(t)$ is modeled as a Ricker wavelet [24].

In order to avoid the use of secondary storage and memory, our RTM code implements the optimal checkpointing strategy, described in [25, 26]. Details of our RTM implementation are shown in Algorithm 1, which is further discussed in Section 6.

6 CSA-based auto-tuning

Katagiri *et al.* [27] defines three types of auto-tuning: i) install-time: when the estimation procedure is affected by machine environments, ii) before execution-invocation: when the estimation procedure is affected by user's knowledge, input parameters or number of processors, for example, and iii) runtime: when the estimation is affected by other parameters generated in

Table 1: CSA parameters used in the numerical experiments.

T_0^{gen}	T_0^{ac}	N	m
0.1	0.9	30	5

runtime. In this paper, we propose a runtime auto-tuning for adequately determining the size of parallel loops subsets to be dynamically distributed among OpenMP threads.

Since the relation between the chunk size of the parallel loops and the total execution time of a program is unknown, the use of a stochastic optimization method is mandatory. This relation is particularly challenging for the FDM because of its stencil. Using a multidimensional stencil means that the access to memory is non-linear at each wave propagation time step, making it more complex to avoid cache misses. For this reason, the proposed auto-tuning employs CSA to find the chunk size that minimizes the execution time.

The CSA parametrization is slightly more straightforward than the SA, but still a challenging task. For all the tests performed in this work, we adopted the following parametrization rules. For the proposed auto-tuning algorithm, we determined, by trial and error, the values of $T_0^{\text{gen}} = 0.1$ and $T_0^{\text{ac}} = 0.9$, for the initial generation and acceptance temperatures, respectively. The number of iterations, N, and the number of SA optimizers, m, influence the convergence and exploration of the solution variables space. Large values of N and m might result in chunk size estimates closer to the global optimum, with the drawback of greater execution times. We found a good compromise with the values $N = 30$ and $m = 5$. The parameters σ_D^2 and α do not need to be configured, they can be kept fixed, in all simulations, according to [12], with $\sigma_D^2 = 0.99\left(\frac{m-1}{m^2}\right)$ and $\alpha = 0.005$. For all the tests that we performed, with different data sets, problem sizes, and machines, the CSA algorithm has shown to be quite robust to the initialization of the parameters. We were able to achieve consistent results by using the same parameter values in all the tests. The CSA configuration parameters used in the experiments are summarized in Table 1.

Four main parallel loops of the RTM are able to have their chunk sizes defined, namely, i) the forward propagation of the source (Line 14 of Algorithm 1), ii) the backward propagation of the observed data (Line 24 of Algorithm 1), iii) the insertion of the receivers data (Line 28 of Algorithm 1) and iv) the image condition (Line 33 of Algorithm 1). The optimal checkpointing strategy (Line 31 of Algorithm 1) recomputes some of the forward propaga-

tion time steps and can also have its chunk size defined by an auto-tuning method.

Since the three propagation loops are essentially the same, we only apply the proposed auto-tuning for the forward propagation. The chunk size obtained is then applied to the forward propagation, the backward propagation and the checkpointing. On the other hand, the receivers insertion and image condition loops are not auto-tuned. These loops have a significantly smaller dimension, in comparison with the propagation loops. In our tests, these loops together spent less than 2% of the total execution time. Furthermore, they mostly perform linear access to memory, which is ideal for a static distribution. Its overhead may overcome the benefit of auto-tuning the receivers data insertion and image condition loops. As shown in Algorithm 1 (Line 9), the proposed auto-tuning is performed only for the first shot. All the following shots use the same chunk size computed for the first shot.

Algorithm 2 details the implementation of the proposed auto-tuning. The initial set of solutions (chunk sizes) is randomly chosen in the interval $[50, N_{\text{loop}}/N_{\text{threads}}]$. We disregarded small chunk sizes because of the high overhead to dynamically schedule them. Chunk sizes greater than the chunk size of the standard *static* distribution ($N_{\text{loop}}/N_{\text{threads}}$) are also not taken into consideration because they would lead to the number of blocks less or equal than the number of threads and thus, the distribution would be forced to be static.

For each CSA iteration, each optimizer only measures the execution time of the first time step in the forward propagation, using its current chunk size (Lines 6 and 13). As shown in [11], the runtime of the first time step can accurately represent the total propagation execution time. This first-time step is performed twice (Line 4) and only the elapsed time of the second repetition is registered (Lines 5 and 12) in order to avoid cache population effects. The CSA then uses those time measures as the cost function values and generates the next set of solutions (Line 17).

7 Numerical experiments

Our experiments were conducted on 3 different computational environments, namely:

- Leuven: Single compute node hosting four sixteen-core AMD Opteron (TM) Processor 6376 at 2.3 GHz and 256 GB RAM. This equipment is

Algorithm 1: Reverse Time Migration with auto-tuning. ns is the number of time steps. t_i is the i-th time step in the RTM algorithm.

```
1: distribute shots among nodes using MPI
2: read RTM parameters
3: initialize checkpointing variables
4: compute absorbing boundaries coefficients
5: initialize auto-tuning parameters
6: #OpenMP parallel section begin
7: for all shots location do
8:    read shot seismogram
9:    if it is the first shot then
10:      autotuning() (See Algorithm 2)
11:   end if
12:   for (t_i = 0 to ns) do
13:      #OpenMP parallel loop using the auto-tuned chunk size in a
         dynamic distribution
14:      for all grid points do
15:         compute the wavefield
16:      end for
17:      add the source wavelet
18:      if (t_i is a checkpoint) then
19:         save Checkpoint
20:      end if
21:   end for
22:   for (t_i = ns - 1 to 0) do
23:      #OpenMP parallel loop using the auto-tuned chunk size in a
         dynamic distribution
24:      for all grid points do
25:         compute the wavefield
26:      end for
27:      #OpenMP parallel loop using static distribution
28:      for all receivers location do
29:         inject observed data samples at time t_i
30:      end for
31:      get forward wavefield at t_i from the checkpoints using the
         auto-tuned chunk size in a dynamic distribution
32:      #OpenMP parallel loop using static distribution
33:      for all main grid points do
34:         perform image condition
35:      end for
36:   end for
37: end for
38: #OpenMP parallel section end
39: reduce all nodes migrated sections
```

Algorithm 2: Proposed auto-tuning method, function *autotuning()* of Algorithm 1. t_i is the i-th time step in the RTM algorithm.

```
1: t_i = 0
2: for all (auto-tuning iterations) do
3:    for all optimizers do
4:       for (i = 1 to 2) do
5:          if (i == 2) then
6:             time measure begin
7:          end if
8:          #OpenMP parallel loop using the current chunk size in a
            dynamic distribution
9:          for all grid points do
10:            compute the wavefield
11:         end for
12:         if (i == 2) then
13:            time measure end
14:         end if
15:      end for
16:   end for
17:   CSA generates a new solution for each optimizer from the time
      measures
18: end for
19: return the solution with the lowest cost function
```

located at the Universidade Federal do Rio Grande do Norte (UFRN).

- NPAD: 68 compute nodes. Each compute node hosts two CPUs Intel Xeon Sixteen-Core E5-2698v3 at 2.3 GHz and 128 GB RAM DDR4 2133. It is equipped with a 60 TB Lustre parallel distributed file system. This equipment is located at the High-Performance Computing Center at UFRN (NPAD/UFRN).

- Yemoja: 860 compute nodes. Each compute node hosts two 10-core Intel Xeon E5-2690 Ivy Bridge v2 at 3 GHz. 200 nodes with 256 GB of RAM and 656 nodes with 128 GB RAM. It is equipped with an 850 TB Lustre parallel distributed file system. This equipment is located at the Manufacturing and Technology Integrated Campus of the National Service of Industrial Training (SENAI CIMATEC).

In order to validate the 3D acoustic wave propagator used in our RTM program, we compared a seismic trace computed by our program with the 3D acoustic analytical solution, computed based on [28], in a homogeneous velocity model. Fig. 1 shows that our wave propagator provides an accurate approximation to the analytical solution of the 3D acoustic wave equation. The waveform of both curves is essentially the same, as well as the amplitudes.

For all the following tests, $f_{\text{peak}} = 20$ Hz, the time sampling is 1 ms, the number of time steps is 3501, the spatial resolutions are $\Delta x_1 = \Delta x_2 = \Delta x_3 =$ 10 m and the absorbing border thickness is 50 points in all directions of the 3D mesh. We built $c(\mathbf{x})$ by using a two layers model with a flat interface positioned at the center of the vertical dimension, where the top and bottom layers have velocities of 1400 m/s and 2000 m/s, respectively. The number of buffers (n_{b}) and checkpoints (n_{c}) depends on the size of the input, as shown in Table 2. The numbers of buffers were chosen in order to use up to 128 GB of RAM. The numbers of checkpoints are optimal, according to [26].

The first set of experiments compares the performance of the proposed auto-tuning method and the OpenMP *auto* and *static* schedules, performing RTM of a single seismic shot, in different computational resources.

As seen in Fig. 2, the proposed auto-tuning strategy outperforms the *auto* and *static* schedules in this set of experiments. The proposed method speedups were 5.2% and 8.1%, compared with the *auto* and *static* schedules, respectively, on Yemoja. Regarding the tests performed in Leuven, the pro-

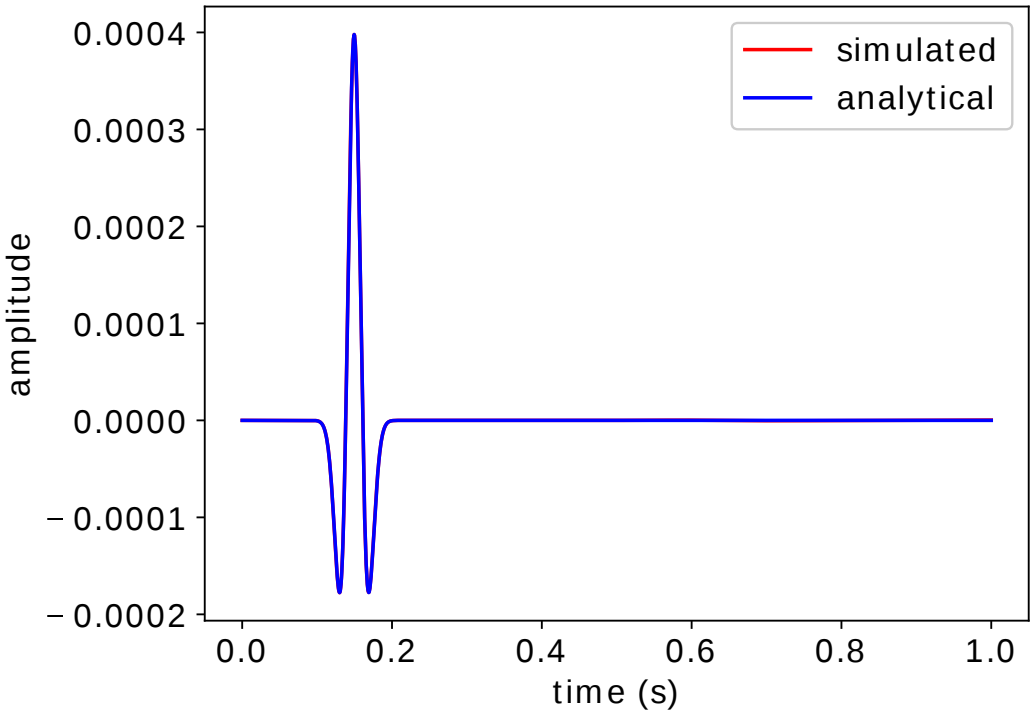

Figure 1: Seismic traces (blue) from the analytical solution and (red) from our wave propagator. The source is a Ricker wavelet with peak frequency of 20 Hz. The distance between source and receiver is 200 m. The medium has a constant velocity of 2000 m/s.

Table 2: Number of buffers and checkpoints used in the experiments as function of the input size. The input size does not include the absorbing border. n_1, n_2 and n_3 are the number of samples for the spatial dimensions x_1, x_2 and x_3, being the latter the vertical dimension.

Input size ($n_1 \times n_2 \times n_3$)	n_b	n_c
$201 \times 401 \times 401$	170	3330
$401 \times 401 \times 401$	100	3400
$801 \times 401 \times 401$	56	1848

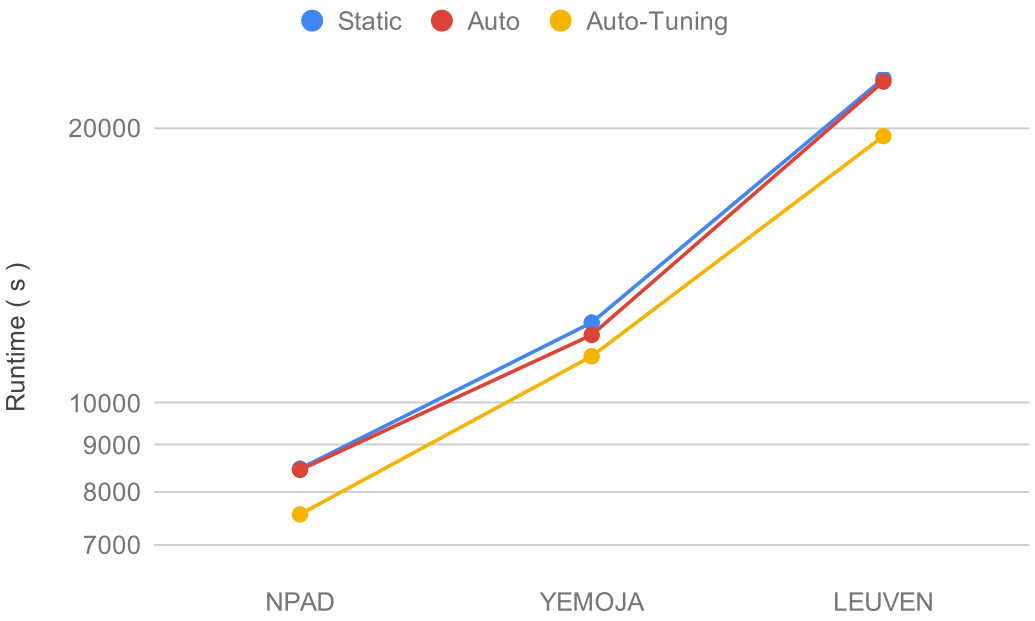

Figure 2: Single shot RTM runtime for the proposed auto-tuning, compared with the auto and the static scheduling types, in 3 different machines, namely NPAD, Yemoja and Leuven. These tests were performed with an input size of $(n_1 \times n_2 \times n_3) = 401 \times 401 \times 401$. Each point is a median of at least 5 executions.

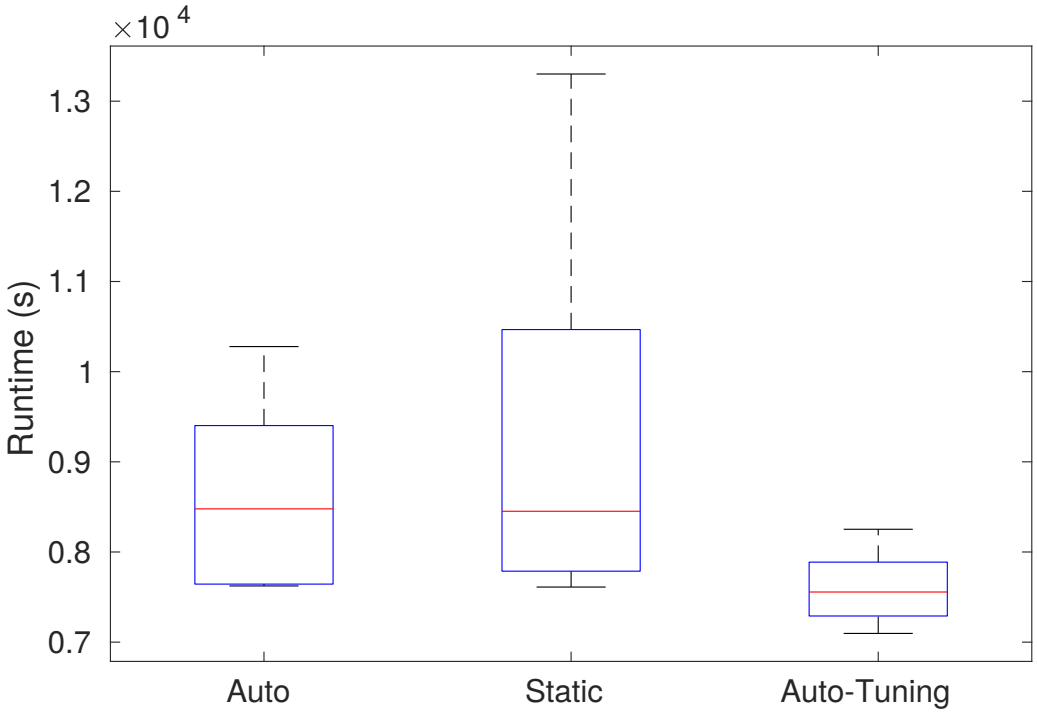

Figure 3: Single shot RTM runtime for the proposed auto-tuning, compared with the auto and the static scheduling types. These tests were performed at NPAD for an input size of $(n_1 \times n_2 \times n_3) = 401 \times 401 \times 401$. Each box plot represents a set of 10 executions.

posed method speedups were 12.8% and 13.5%, compared with the *auto* and *static* schedules, respectively.

Since Leuven has more core units per node, its maximum chunk size ($N_{\text{loop}}/N_{\text{threads}}$) is smaller than it is for NPAD and Yemoja. This fact leads to a significantly smaller search domain for the CSA and might be the reason behind the improved auto-tuning performance, in this platform.

Fig. 3 shows detailed results obtained on NPAD. It shows that, in this particular case, the slowest execution time of the proposed auto-tuning method is faster than the median execution time of both the *auto* and the *static* schedules.

On NPAD, taking the median of 10 executions, the proposed auto-tuning method speedup was 10.6% when compared with the *auto* scheduling, for the RTM of a single seismic shot. When comparing with the *static* scheduling,

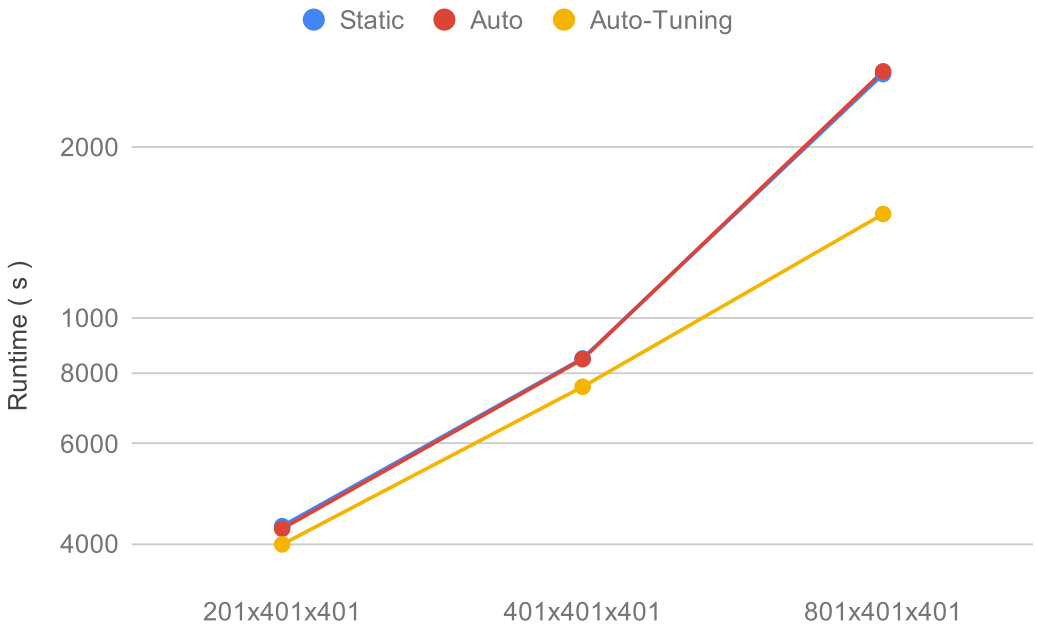

Figure 4: Single shot RTM runtime for the proposed auto-tuning, compared with the auto and the static scheduling types, for 3 different input sizes, namely $201 \times 401 \times 401$, $401 \times 401 \times 401$ and $801 \times 401 \times 401$. These tests were performed at NPAD. Each point is a median of at least 5 executions.

its speedup was 10.9%, also for the RTM of a single seismic shot.

The second set of experiments compares the performance of the proposed auto-tuning method and the OpenMP *auto* and *static* schedules performing a single shot RTM, for different input sizes.

Fig. 4 shows that the proposed auto-tuning strategy outperforms the *auto* and *static* scheduling types, in this set of experiments. The proposed method speedups were 6.14% and 7.14%, compared with the *auto* and *static* scheduling types, respectively, for an input size of $201 \times 401 \times 401$. When tests were performed for an input size of $401 \times 401 \times 401$, the proposed method speedups were 10.6% and 10.9%, compared with the *auto* and *static* scheduling types, respectively. Finally, for an input size of $801 \times 401 \times 401$, the proposed method speedups were 44% and 43.3%, compared with the *auto* and *static* scheduling types, respectively.

The larger the input size, the bigger the chunks of the static distribution. For the input sizes of $201 \times 401 \times 401$, $401 \times 401 \times 401$, and $801 \times 401 \times$

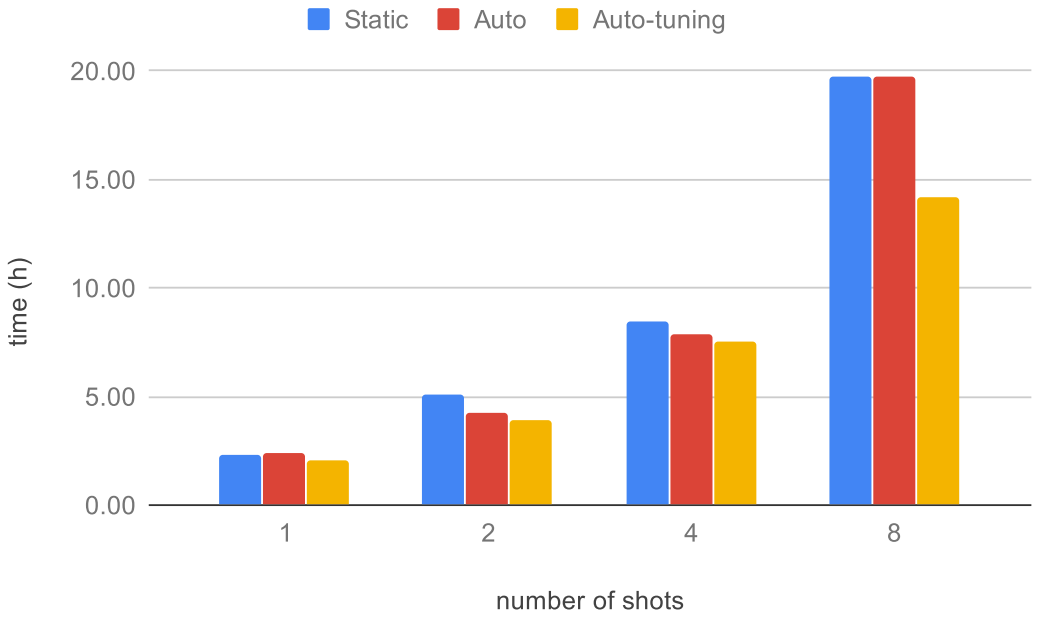

Figure 5: Multiple shots RTM runtime for the proposed auto-tuning, compared with the auto and the static scheduling types. For each amount of shots, all shots were migrated in a single node. These tests were performed at NPAD for an input size of $(n_x, n_y, n_z) = 401 \times 401 \times 401$. Each bar represents a set of at least 5 executions.

401, the chunk size of the static distribution are 9, 15, and 27 millions of loop iterations. By working with larger chunks, data locality of the static distribution reduces, which explains its performance decrease for larger input sizes.

On the other hand, for the same input sizes, the median of the chunk sizes chosen by the proposed auto-tuning were 71, 264 and 130 thousands of loop iterations. By processing smaller chunks, the set of data being processed by all cores at a time are physically closer. This data locality increases the reuse of the data in cache memory.

The third set of experiments compares the performance of the proposed auto-tuning method and the OpenMP *auto* and *static* scheduling types, performing RTM in multiple seismic shots. For this test, sets of 1, 2, 4 and 8 shots were migrated, in a single node. In case of using multiple nodes, the same strategy would be replicated at each node.

The proposed auto-tuning method outperforms the *auto* and the *static*

schedules for all the tested number of shots. As shown in Fig. 5 for the RTM of multiple shots, since the proposed auto-tuning is performed only a single time and the resulting chunk size is used in the parallelization of all the shots, its relative overhead reduces as the number of shots increases. This fact causes the highest speedups of the proposed auto-tuning to be achieved for the highest number of shots tested. In this scenario, when 8 shots were migrated, the proposed auto-tuning speedups were 28.4% and 28.3%, compared with the *auto* and *static* schedules.

8 Conclusions

We have proposed a CSA-based auto-tuning strategy for properly choosing the optimal chunk size that reduces the execution time of a 3D reverse time migration algorithm, implemented in parallel with OpenMP. The proposed approach is designed to work wherever the code is executed, being robust for changes in computational environment parameters, such as the number of threads, processors, RAM, and compiler.

Experiments of auto-tuning the RTM of a single seismic shot have shown that the proposed auto-tuning outperforms OpenMP *auto* and *static* scheduling types when using different input sizes and computational resources. In this case, the proposed auto-tuning reached speedups up to 44%. The proposed method presents better results for larger inputs, which improves the parallel scalability of 3D RTM.

We have also extended the proposed method to auto-tune the RTM of multiple seismic shots, by just reusing the chunk size obtained in the first shot of each node to the following shots migration. In this case, the proposed auto-tuning reached speedups up to 28.4%. For all the number of shots used. the proposed auto-tuning method outperformed the *auto* and *static* OpenMP schedules.

Different strategies for auto-tuning the 3D RTM of multiple shots, as well as the influence of the CSA parameters on the proposed auto-tuning technique are matters of further research.

9 ACKNOWLEDGMENTS

The authors gratefully acknowledge support from Shell Brazil through the project "*Novos Métodos de Exploração Sísmica por Inversão Completa das Formas de Onda*" at the Universidade Federal do Rio Grande do Norte (UFRN) and the strategic importance of the support given by ANP through the R&D levy regulation. The authors are also thankful to CNPq (*Conselho Nacional de Desenvolvimento Científico e Tecnológico*) and CAPES (*Coordenação de Aperfeiçoamento de Pessoal de Nível Superior*) for partially funding this research and to the High-Performance Computing Center at UFRN (NPAD/UFRN) and the Manufacturing and Technology Integrated Campus of the National Service of Industrial Training (SENAI CIMATEC) for making computer resources available. Finally, the authors thank Jorge Lopez from Shell for reviewing and providing important comments on this paper.

References

[1] E. Baysal, D. D. Kosloff, and J. W. C. Sherwood, "Reverse time migration," *Geophysics*, vol. 48, no. 11, pp. 1514–1524, 1983.

[2] D. D. Kosloff and E. Baysal, "Migration with the full acoustic wave equation," *Geophysics*, vol. 48, no. 6, pp. 677–687, 1983.

[3] J.-H. Zhang, S.-Q. Wang, and Z.-X. Yao, "Accelerating 3D Fourier migration with graphics processing units," *GEOPHYSICS*, 2009.

[4] M. Araya-Polo, F. Rubio, R. De La Cruz, M. Hanzich, J. M. Cela, and D. P. Scarpazza, "3D seismic imaging through reverse-time migration on homogeneous and heterogeneous multi-core processors," *Scientific Programming*, 2009.

[5] D. A. Nunes-Do-Rosário, S. Xavier-De-Souza, R. C. Maciel, and J. C. Costa, "Parallel Scalability of a Fine-Grain Prestack Reverse Time Migration Algorithm," *IEEE Geoscience and Remote Sensing Letters*, 2015.

[6] M. Tchiboukdjian, V. Danjean, T. Gautier, F. Le Mentec, and B. Raffin, "A work stealing scheduler for parallel loops on shared cache multi-

cores," in *Lecture Notes in Computer Science (including subseries Lecture Notes in Artificial Intelligence and Lecture Notes in Bioinformatics)*, 2011.

[7] E. L. Padoin, M. Castro, L. L. Pilla, P. O. A. Navaux, and J. Méhaut, "Saving energy by exploiting residual imbalances on iterative applications," in *2014 21st International Conference on High Performance Computing (HiPC)*, 2014, pp. 1–10.

[8] E. L. Padoin, L. L. Pilla, M. Castro, P. O. Navaux, and J. F. Méhaut, "Exploration of load balancing thresholds to save energy on iterative applications," in *Communications in Computer and Information Science*, 2017.

[9] T. Katagiri, S. Ohshima, and M. Matsumoto, "Auto-tuning of computation kernels from an FDM code with ppOpen-AT," in *Proceedings - 2014 IEEE 8th International Symposium on Embedded Multicore/Manycore SoCs, MCSoC 2014*, 2014.

[10] ——, "Directive-Based Auto-Tuning for the Finite Difference Method on the Xeon Phi," in *Proceedings - 2015 IEEE 29th International Parallel and Distributed Processing Symposium Workshops, IPDPSW 2015*, 2015.

[11] T. Barros, J. B. Fernandes, I. A. Souza-de Assis, and S. Xavier-deSouza, "Auto-Tuning of 3D Acoustic Wave Propagation in Shared Memory Environments," in *First EAGE Workshop on High Performance Computing for Upstream in Latin America*. Santander: EarthDoc, 2018. [Online]. Available: http://www.earthdoc.org/publication/publicationdetails/?publication=94579

[12] S. Xavier-de Souza, J. A. K. Suykens, J. Vandewalle, and D. Bolle, "Coupled Simulated Annealing," *IEEE Transactions on Systems, Man, and Cybernetics, Part B (Cybernetics)*, vol. 40, no. 2, pp. 320–335, 2010.

[13] A. C. Sena, A. P. Nascimento, C. Boeres, V. Rebello, and A. Bulcão, "An approach to optimise the execution of RTM algorithm in multicore machines," in *Proceedings - 2011 7th IEEE International Conference on eScience, eScience 2011*, 2011.

[14] C. Andreolli, P. Thierry, L. Borges, C. Yount, and G. Skinner, "Genetic Algorithm Based Auto-Tuning of Seismic Applications on Multi and Manycore Computers," in *EAGE Workshop on High Performance Computing for Upstream*, 2014.

[15] C. Andreolli, P. Thierry, L. Borges, G. Skinner, and C. Yount, "Characterization and Optimization Methodology Applied to Stencil Computations," in *High Performance Parallelism Pearls*, J. Jeffers and J. Reinders, Eds. Boston: Elsevier, 2015, ch. 23, pp. 377–396. [Online]. Available: http://www.sciencedirect.com/science/article/pii/B9780128021187000236

[16] L. Dagum and R. Menon, "OpenMP: an industry standard API for shared-memory programming," *IEEE Computational Science and Engineering*, vol. 5, no. 1, pp. 46–55, Jan 1998.

[17] J. M. Carcione, G. C. Herman, and A. P. E. ten Kroode, "Seismic modeling," *Geophysics*, 2002.

[18] C. Cerjan, D. Kosloff, R. Kosloff, and M. Reshef, "A nonreflecting boundary condition for discrete acoustic and elastic wave equations," p. 705, 1985.

[19] Ö. Yilmaz, *Seismic Data Analysis: Processing, Inversion, and Interpretation of Seismic Data*, ser. Investigations in geophysics. Society of Exploration Geophysicists, 2001, no. v. 2.

[20] L. Clarke, I. Glendinning, and R. Hempel, "The MPI message passing interface standard," in *Programming Environments for Massively Parallel Distributed Systems*, K. M. Decker and R. M. Rehmann, Eds. Basel: Birkhäuser Basel, 1994, pp. 213–218.

[21] S. Kirkpatrick, C. D. Gelatt, and M. P. Vecchi, "Optimization by simulated annealing," *Science*, vol. 220, no. 4598, pp. 671–680, 1983.

[22] K. Gonçalves-e Silva, D. Aloise, and S. Xavier-de Souza, "Parallel synchronous and asynchronous coupled simulated annealing," *The Journal of Supercomputing*, vol. 74, no. 6, pp. 2841–2869, 2018.

[23] K. Gonçalves-e Silva and S. Xavier-de Souza, "Perpetual orbit coupled simulated annealing for continuous optimization," *arXiv preprint arXiv:1803.01059*, 2018.

[24] Y. Wang, "Frequencies of the Ricker wavelet," *Geophysics*, vol. 80, no. 2, pp. A31–A37, 2015.

[25] W. Symes, "Reverse time migration with optimal checkpointing," *Geophysics*, 2007.

[26] A. Griewank and A. Walther, "Algorithm 799: revolve: an implementation of checkpointing for the reverse or adjoint mode of computational differentiation," *ACM Transactions on Mathematical Software*, 2000.

[27] T. Katagiri, K. Kise, H. Honda, and T. Yuba, "Fiber: A generalized framework for auto-tuning software," in *High Performance Computing*, A. Veidenbaum, K. Joe, H. Amano, and H. Aiso, Eds. Berlin, Heidelberg: Springer Berlin Heidelberg, 2003, pp. 146–159.

[28] A. De Hoop, "A modification of Cagniard's method for solving seismic pulse problems," *Applied Scientific Research, Section B*, vol. 8, no. 1, pp. 349–356, 1960.